Interfacial antiferromagnetic coupling and high spin polarization in metallic phthalocyanines

Junwei Tong,[1] Feifei Luo,[1] Liuxia Ruan,[1] Guohuai Liu,[2] Lianqun Zhou,[3] Fubo Tian,[4] Gaowu Qin,[1] and Xianmin Zhang[1,*]

[1]*Key Laboratory for Anisotropy and Texture of Materials (Ministry of Education), School of Material Science and Engineering, Northeastern University, Shenyang 110819, China*

[2]*The State Key Lab of Rolling and Automation, Northeastern University, Shenyang 110819, China*

[3]*Suzhou Institute of Biomedical, Engineering and Technology, Chinese Academy of Sciences, Suzhou 215163, China*

[4]*State Key Laboratory of Superhard Materials, College of Physics, Jilin University, Changchun 130012, China*

(Received 3 August 2020; revised 13 October 2020; accepted 6 January 2021; published 20 January 2021)

Exploration and understanding of the spinterface between magnetic electrodes and organic semiconductors are vital to get an insight into interfacial science and develop spintronic devices. Intrigued by the fact that the modification of chemical states may affect interfacial exchange coupling, magnetic interactions between a series of metallic phthalocyanines (*M*Pcs, M = Cr, Mn, Fe, Co) and surface oxidized Co were studied. Interestingly, these four *M*Pcs are all antiferromagnetically coupled with the Co substrate via the interfacial O atomic layer, but the coupling strength strongly relies on the type of metallic ion in the *M*Pcs. The physical mechanism for different exchange strengths is explored and discussed in terms of a superexchange model via O atoms. It is also noted that the adsorption energy and work function of the surface oxidized Co were sensitive to the metallic ions of *M*Pcs. The valence and spin state of central 3*d* metallic ions could be tuned by the surface oxidized Co. Very interestingly, high negative spin-polarized spinterfaces are obtained in these *M*Pcs. The spin polarizations are up to −86% and −80% for CrPc and MnPc, respectively. Additionally, high spin polarization can be maintained beyond room temperature because of the very large interfacial coupling energy, demonstrating a promising application of *M*Pcs in spintronic devices.

DOI: 10.1103/PhysRevB.103.024435

I. INTRODUCTION

Molecules deposited on metal surfaces are currently of particular interest due to their extensive applications in physical electronics [1–5]. As one of the typical organic semiconductors, phthalocyanines (Pcs) are conjugated macrocycles with 18π electrons, which have been widely studied in organic electronics and spintronics [2,6–13]. The adsorption of Pcs could modify the magnetic properties of both molecules and ferromagnetic (FM) substrates through interfacial coupling by forming spinterfaces [1,14–21]. The temperature dependence of spin polarization (SP) at the spinterface is strongly related to the magnitude of coupling strength [22–30] because the magnetic exchange coupling of spin in magnetic molecules with a FM substrate determines the magnetic order of paramagnetic molecules [25,31]. A weak exchange interaction cannot maintain the magnetic order of paramagnetic molecules on the FM substrate [25], which may be responsible for the low SP in the organic/FM spinterface at room temperature. Thus, seeking a strong coupling between magnetic molecules and FM substrate and understanding the inner physical mechanism are vital for developing advanced organic spintronics. It has been reported that the interactions between metallic Pc and substrate could be used to manipulate the spin state of metallic Pcs [2,4,6,32]. The easy axis of magnetization for FePc tuned by the O atomic layer as deposited on Cu(110) has been demonstrated [3,4]. The magnetic coupling between FePc and Co films could also be changed by surface oxidation [33,34]. These studies demonstrate the interfacial interactions are very interesting in affecting the spinterface. The electronic structures of metallic Pcs (*M*Pcs) are strongly dependent on their central metallic ions [35–37], which provides an effective way to investigate the interaction between *M*Pcs and FM surfaces [2,6,7].

Here, intrigued by the fact that the modification of chemical states may affect the interfacial exchange coupling of molecules/FM systems, the magnetic interaction between *M*Pcs (M = Cr, Mn, Fe, Co) and Co through the interfacial O atomic layer was studied using first-principles calculations. It is noted that these four *M*Pcs are all antiferromagnetically (AFM) coupled to the Co substrate through the interfacial O atomic layer. The size of the magnetic coupling strength strongly depends on the type of central atom in the *M*Pcs. The physical mechanism for the different exchange strengths was explored and discussed by a superexchange model via O atoms. Furthermore, it is found that both the valence change of 3*d* metal ions in *M*Pcs and the work function of the surface oxidized Co are sensitive to the central atoms, meaning that the modification of the central metal atom in *M*Pcs is an effective way to design a functional spinterface. Most interestingly, high negative spin-polarized spinterfaces are obtained in these *M*Pcs. The SPs are up to −86% and −80% for CrPc and MnPc, respectively, showing a promising application of *M*Pcs in spintronic devices.

II. COMPUTATIONAL DETAILS

First-principles calculations were performed based on the density functional theory (DFT) using the Vienna *ab*

*zhangxm@atm.neu.edu.cn

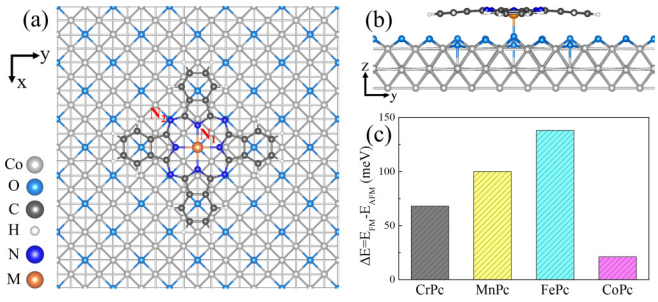

FIG. 1. (a) Top view of *M*Pcs on $c(2 \times 2)$O/Co(001). *M*Pcs adsorbed on the on-top-of-O position (M = Cr, Mn, Fe, and Co). (b) Side view. Orange, blue, dark gray, white, light blue, and light gray represent the central metal, N, C, H, O, and Co atoms, respectively. N_1 is the direct bond to the central metal atom of *M*Pcs rather than the N_2. The coordinate system is shown in the left of (a) and (b). (c) The energy difference for AFM and FM coupled *M*Pcs and the Co substrate through O atoms.

initio Simulation Package (VASP) [38,39]. The Perdew-Burke-Ernzerhof of spin-polarized generalized gradient approximation was applied for the exchange and correlation functional [40]. An effective Hubbard term (Dudarev's method) of $U_{\text{eff}} = 3\,\text{eV}$ was included for the $3d$ orbitals of the metal center [2,33,34,41]. The van der Waals interactions proposed by Grimme (DFT-D2) were included in the calculations to incorporate the long-range dispersion forces in the molecule system [42]. The energy cutoff was set as 400 eV, and a Γ-point-only k mesh was used [33]. Except for the bottom Co layer, all atomic positions were relaxed until the forces were smaller than $0.02\,\text{eV/Å}$. The postprocessing of VASP data was performed using VASPKIT code [43].

III. RESULTS AND DISCUSSION

A. Interfacial magnetic coupling and charge transfer

The face-centered cubic (fcc) Co was used for calculation, and the optimized lattice constant was 3.517 Å, which agrees with previous papers [44,45]. The substrate contained 3 monolayers (MLs) of Co film. A well-characterized $c(2 \times 2)$ superstructure of 0.5-ML atomic oxygen on top of the Co film was used to simulate the surface oxidized Co, which has been experimentally achieved on the Co(001) surface [34,46,47]. The *M*Pcs were on top of the oxygen atom, as shown in Figs. 1(a) and 1(b). Both our calculations (see Fig. S1 in the Supplemental Material) [48] and previous papers [33,34] show this configuration was the ground state. The spin in *M*Pcs would be coupled to the Co substrate through the oxygen atom. To study the magnetic interaction, the energies for AFM (E_{AFM}) and FM (E_{FM}) coupled *M*Pcs and the Co substrate were calculated. The energy difference is defined as $\triangle E = E_{\text{FM}} - E_{\text{AFM}}$. Thus, the negative and positive $\triangle E$ correspond to FM and AFM coupling, respectively [49]. As shown in Fig. 1(c), it was found that E_{FM} was larger than E_{AFM}. This indicates all these *M*Pcs were AFM coupled to the Co substrate independent of the metallic ion. The exchange energy varies from 21 to 138 meV for different *M*Pcs. The large change of exchange energy means the central atoms of *M*Pcs provide an effective way to tune the magnetic interaction between *M*Pcs and the Co substrate.

The spin-charge densities for MnPc and MnPc absorbed on $c(2 \times 2)$O/Co(001) are shown here to discuss the interaction between MnPc and surface oxidized Co, and a similar investigation of CrPc, FePc, and CoPc in detail can be found in the Supplemental Material (Figs. S2–S4) [48]. The isosurface spin-charge densities of AFM and FM coupled MnPc and Co are shown in Figs. 2(a) and 2(b), respectively. It was found that the surface O atoms were magnetized due to interaction with the Co substrate. The spin charge in MnPc was almost located in the Mn ion and N_1 atoms. The magnetic moments of the Mn ion and N_1 were AFM coupled regardless of the magnetic exchange between MnPc and the Co substrate. The spin-charge density of MnPc in the xy plane crossing the central Mn ion for the isolated MnPc molecule, AFM coupled MnPc and Co, and FM coupled MnPc and Co are shown in Figs. 2(c), 2(d), and 2(e), respectively. It is noted that the magnetic moments between the Mn ion and N_1 were AFM coupled for all three MnPc cases, which means the magnetism in N_1 atoms was dominated by spin in the Mn ion. However, the magnetism in N_2 was independent of that in the Mn ion, which changes with altering of the magnetic states of MnPc. Due to the interaction with the substrate, it was found that the Pc ring was also magnetized by the presence of spin charge on C and H atoms. The spin charge in the Pc ring was the same for AFM and FM coupled MnPc and the Co substrate, as illustrated in Figs. 2(d) and 2(e), respectively. This denotes that the magnetism in the Pc ring was dominated by the substrate rather than by the central metal atom.

The adsorption of *M*Pcs on the surface of $c(2 \times 2)$O/Co(001) would lead to the charge transfer between *M*Pcs and the $c(2 \times 2)$O/Co(001) substrate, which may change the valence of the central metal ion and influence the magnetic coupling between *M*Pcs and the Co substrate. To illustrate the change transfer, the charge density difference $\Delta\rho$ of *M*Pcs on surface oxidized Co was plotted in Figs. 3(a) and 3(b), which was calculated by $\Delta\rho = \rho_{M\text{Pc/O/Co(001)}} - \rho_{\text{O/Co(001)}} - \rho_{M\text{Pc}}$, where $\rho_{M\text{Pc/O/Co(001)}}$, $\rho_{\text{O/Co(001)}}$, and $\rho_{M\text{Pc}}$ are the charge densities of the *M*Pc on $c(2 \times 2)$O/Co(001), $c(2 \times 2)$O/Co(001) substrate, and an isolated *M*Pc molecule, respectively. The plane-averaged charge density difference along the z direction is shown in the left of Fig. 3(a). It was found that the charge in *M*Pcs was depleted and accumulated at the interface, respectively. The magnitude of charge redistribution at the interface was dependent on the metallic ions of *M*Pcs. The MnPc shows the strongest charge transfer, and CoPc shows the weakest charge transfer. The magnitudes of charge transfer for CrPc and FePc were almost the same. The isosurface charge density difference of MnPc on the surface oxidized Co is shown in the right of Fig. 3(a). The charge transfer existed on the whole MnPc. The molecular configuration of the MnPc molecule bent due to the strong interaction with the surface oxidized Co. The charge density difference in the xz plane crossing the central metal atoms of different *M*Pcs is illustrated in Fig. 3(b). It was found that most of the charge transfer is from the central metal atoms of *M*Pcs. All *M*Pcs show a charge accumulation in the middle of the central metal ion and the O atom, indicating the formation of chemical bonds

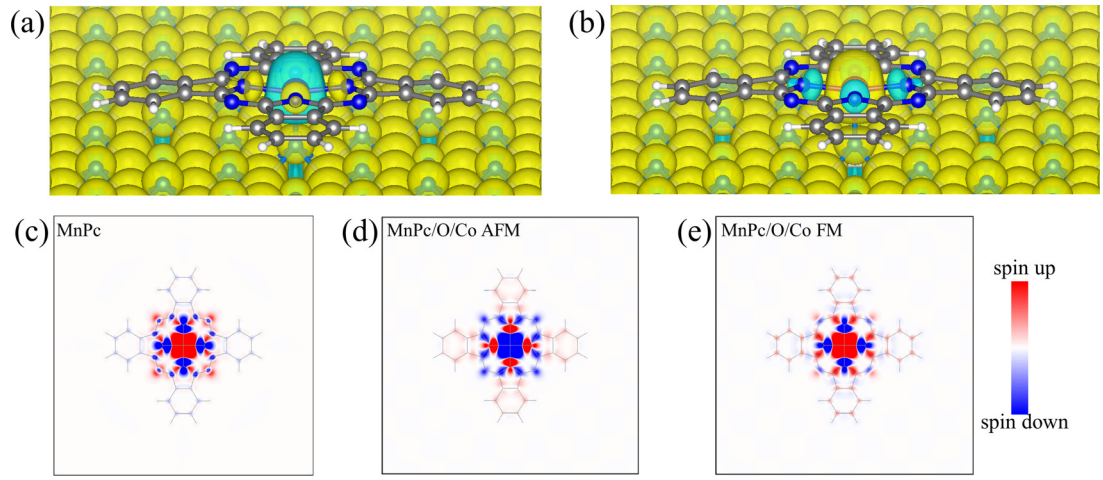

FIG. 2. Spin-charge density for MnPc and MnPc on $c(2 \times 2)$O/Co(001). (a) Isosurface spin-charge density for AFM coupled MnPc and Co; (b) FM coupled MnPc and Co. Yellow and blue denote spin-up and spin-down charges, respectively. The isosurface level was $0.02\,\mathrm{e}/\text{Å}^3$. (c) Spin-charge density of MnPc in the xy plane crossing the Mn atom for the MnPc molecule; (d) AFM coupled MnPc and Co; (e) FM coupled MnPc and Co. Red and blue denote spin-up and spin-down charges, respectively.

[3]. Based on the method of Bader's charge analysis [50–52], the central Cr, Mn, Fe, and Co atoms in *M*Pcs transfer 0.30, 0.13, 0.30, and 0.04 electrons, respectively, to the oxygen atoms after adsorption on surface oxidized Co. Moreover, the shapes of charge depletion and accumulation strongly depend on the central metal ions, implying their electrons' occupation of d orbitals may change after adsorption of *M*Pcs on $c(2 \times 2)$O/Co(001). The charge transfer between *M*Pcs and surface oxidized Co would induce the formation of a dipole moment at the interface [2,53,54]. The dipole moment ($\delta\mu$) could be calculated by the following formula [53]:

$$\delta\mu(z) = \int_{z_c}^{z_c+z} z' \int_0^b \int_0^a \Delta\rho(x, y, z')dxdydz', \qquad (1)$$

where z_c is the center of the vacuum region, and a and b are the unit cell lattice parameters along the x and y axes, respectively. The positive and negative values indicate dipoles oriented along $-z$ and z, respectively. The dipole moment at the interface would change the surface work function, which influences the electron transport [53–55]. According to the Helmholtz equation, the change of the work function $\delta\Phi$ could be estimated by the following formula [in atomic units (a.u.)] [53,56]:

$$\delta\Phi = 4\pi \frac{C}{A_0}\delta\mu, \qquad (2)$$

where C is the fractional coverage and A_0 the area of the surface unit cell (in units of bohr^2). The left of Fig. 3(a) shows a charge transfer from the *M*Pcs to the interface, resulting in the negative dipole moments. Thus, the adsorptions of *M*Pcs reduced the work function of the surface oxidized Co. The plane-averaged electrostatic potential along the direction perpendicular to the interface is illustrated in Fig. 3(c), from which the work function of the Co surface (Φ_{Co}) and the surface covered by MnPc (Φ_{MnPc}) could be obtained. The summary of the work function for the surface covered by *M*Pcs is shown in Fig. 3(d). The absorption of MnPc and CoPc on the surfaces shows the lowest and highest work functions, respectively, while the work functions for the absorption of CrPc and FePc are very close. From Eqs. (1) and (2), the more interface charge transfers, the bigger decrease of the work function [53], agreeing with the results in the left of Fig. 3(a). In addition, the adsorption energy E_{ads} of the *M*Pcs was calculated by $E_{\mathrm{ads}} = E_{\mathrm{O/Co(001)}} + E_{M\mathrm{Pc}} - E_{M\mathrm{Pc/O/Co(001)}}$,

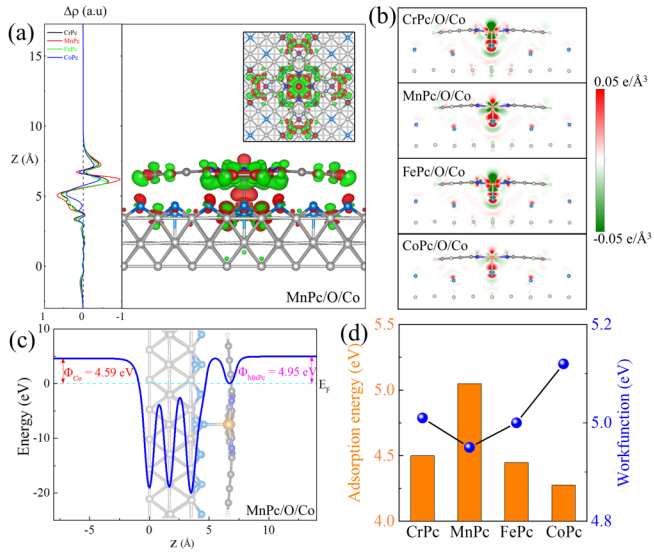

FIG. 3. (a) Left: Plane-averaged charge density difference along the direction perpendicular to the interface (the z direction). Right: Isosurface charge density difference of MnPc on $c(2 \times 2)$O/Co(001). Insert shows the top view of the charge density difference for MnPc on $c(2 \times 2)$O/Co(001). The isosurface level was $0.02\,\mathrm{e}/\text{Å}^3$. Green and red regions show charge depletion and accumulation, respectively. (b) Charge density difference of *M*Pcs on $c(2 \times 2)$O/Co(001) in the xz plane crossing the central metal atoms. (c) Plane-averaged electrostatic potential along the z direction for MnPc/$c(2 \times 2)$O/Co(001). Here, Φ_{Co} and Φ_{MnPc} are the work functions of the Co surface and the surface with the MnPc molecule, respectively. The background shows the corresponding structure. (d) Adsorption energy and work function of *M*Pcs on $c(2 \times 2)$O/Co(001).

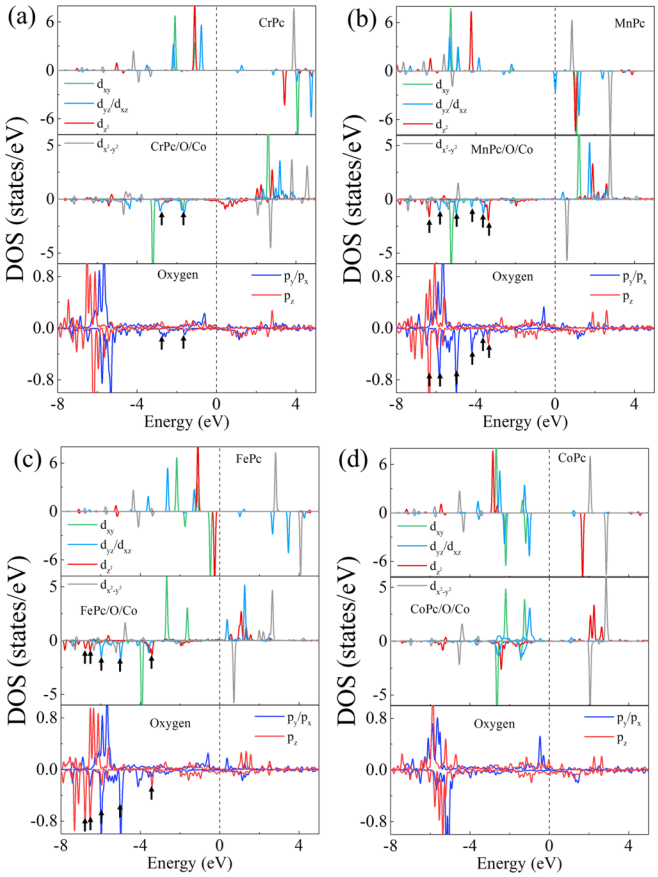

FIG. 4. Projected density of states (PDOS) of the central metal ion and O atoms. (a) Up: PDOS for central Cr 3*d* orbitals of an isolated CrPc molecule; middle: PDOS for central Cr 3*d* orbitals of CrPc on $c(2 \times 2)$O/Co(001); down: PDOS for the 2*p* orbitals of the O atom, which is just below the Cr atom of CrPc on $c(2 \times 2)$O/Co(001). (b) MnPc. (c) FePc. (d) CoPc. The PDOS in the middle and bottom are from the AFM coupled *M*Pcs and the Co substrate. The consistent PDOS peaks for the central metal ion and the O atom are denoted by black arrows.

where $E_{\mathrm{O/Co(001)}}$, $E_{M\mathrm{Pc}}$, and $E_{M\mathrm{Pc/O/Co(001)}}$ are the energies of the $c(2 \times 2)$O/Co(001) substrate, an isolated *M*Pc molecule, and *M*Pc on the the $c(2 \times 2)$O/Co(001) system, respectively. The calculated results are shown in Fig. 3(d). It is also shown that the adsorption energy of *M*Pcs is strongly related to the central metal ion. A negative correlation of adsorption energy and work function was observed, which reflects the fact that both rely on the interface charge transfer.

B. Mechanism of AFM coupling

The projected densities of states (PDOSs) for central metal 3*d* orbitals of *M*Pcs, *M*Pcs on $c(2 \times 2)$O/Co(001), and oxygen under *M* ions are shown in Fig. 4. As shown in Fig. 4(a), the sharp peaks of d_{z^2} and d_{yz}/d_{xz} orbitals of the Cr ion in an isolated CrPc molecule were broadened after CrPc absorbed on $c(2 \times 2)$O/Co(001). This results from the strong interaction of CrPc with the surface oxidized Co, and those orbitals extend in the *z* direction. The crystal field of the Cr ion was changed from square planar to square pyramidal after adsorption, which changes the relative energy and electron occupation of *d* orbitals [57]. The charge in the d_{z^2} orbit of the Cr ion in isolated CrPc was lost after CrPc absorbed on $c(2 \times 2)$O/Co(001), which was consistent with the observed charge transfer in Fig. 2(b). The PDOS of the oxygen atom (the one just below the Cr ion) is drawn at the bottom of Fig. 4(a). The PDOS peaks for p_y/p_x orbitals from the O atom are the same positions as that of d_{yz}/d_{xz} orbitals from the Cr ion, meaning a π bond formed between the O atom and the Cr ion, as denoted by black arrows in Fig. 4(a). Based on the superexchange mechanism, the charges in the O atom would virtually transfer to the Cr ion via the π bond, resulting in the energy difference for AFM and FM coupled CrPc and the Co substrate [31,41,58]. As shown in Figs. 4(b) and 4(c), the charge loss of the Mn and Fe ions was mainly from d_{yz}/d_{xz} and d_{z^2} orbitals, respectively. Both π and σ bonds formed between MnPc (FePc) and O atoms. Owing to the loss of charge, the valence state of Cr, Mn, and Fe changed from (II) in isolated *M*Pc molecules to (III) in *M*Pcs absorbed on $c(2 \times 2)$O/Co(001). In contrast, as shown in Fig. 4(d), the occupation of the *d* orbits for the Co ion in CoPc was unchanged after adsorption on $c(2 \times 2)$O/Co(001). Thus, the valence states for the Co ion in both isolated CoPc and absorbed CoPc were (II), agreeing with the observation in Fig. 3(b). Therefore, the different PDOSs of *M*Pcs present the different bonds that are formed between the metal ion and O atoms, which were related to the superexchange interaction through the O atom.

Figure 5 illuminates the superexchange mechanism between MnPc (CoPc) and the Co substrate via the 3O atom. The 3*d* orbitals of the Mn ion and their electron occupations in MnPc on $c(2 \times 2)$O/Co(001) is shown in the left part of Fig. 5(a) based on the results in Fig. 4. The formation of $\pi[(d_{yz}/d_{xz}) - (p_y/p_x)]$ and $\sigma(d_{z^2} - p_z)$ bonds between the Mn ion and the O atom was also illustrated. The electrons in the O atom would virtually transfer to 3*d* orbitals of the Mn ion and the Co substrate. The spin-up d_{yz}/d_{xz} and d_{z^2} orbitals of the Mn ion were occupied. So only the spin-down electrons in the O atom could transfer to 3*d* orbitals of the Mn ion according to the Pauli exclusion principle, as illustrated by the tilted blue arrows in Fig. 5(a) [31,59]. The density of states (DOS) of fcc Co is shown in Fig. 5, whose spin-up states were fully occupied and spin-down states dominate the Fermi surface. To allow the spin-up electrons in the O atom to transfer to the Co substrate as illustrated by the tilted brown arrows, the magnetization of Co should be antiparallel to that of the Mn ion [59]. As a result, both σ and π bonds result in the Mn ion in MnPc AFM coupled to the Co substrate. In Fig. 5(b), it is found that the π bonds do not contribute to the exchange between the Co ion and the oxidized surface Co substrate because both the spin-up and spin-down states of d_{yz} and d_{xz} orbitals for the central Co ion in CoPc are occupied. The σ bond induces the CoPc AFM coupled to the Co substrate. Compared with other *M*Pcs, the interaction between the Co ion and the O atom was relatively weak, as shown in Fig. 3(b). Thus, the transfer integral between the Co ion and the O atom was weaker, inducing the relatively small magnetic coupling energy between CoPc and the Co substrate [31,58,59]. This agrees with the result in Fig. 1(c). The superexchange mechanism for absorbed CrPc and FePc can be found in Fig. S5 in the Supplemental Material [48].

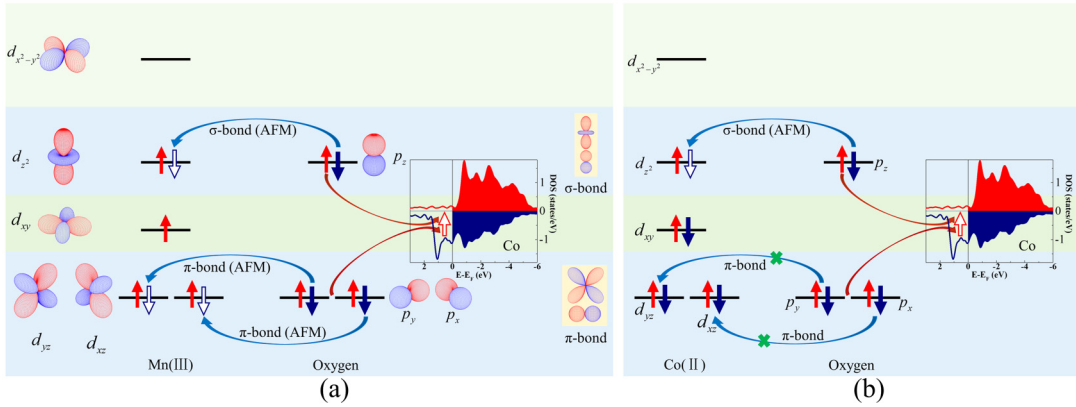

FIG. 5. The superexchange mechanism model via O atoms for MnPc and CoPc. (a) The superexchange mechanism model via O atoms for MnPc. The d_{z^2} orbital of the Mn ion and p_z orbital of the O atom could form the σ bond. The d_{yz}/d_{xz} orbitals and p_y/p_x orbitals would form the π bond. The spin-down electron virtual transfer from O atoms to the $3d$ orbitals of the Mn ion through the σ and π bonds is indicated by the tilted blue arrows. The spin-up electron virtual transfer from O atoms to the Co substrate is indicated by the tilted brown arrows. (b) The superexchange mechanism model via O atoms for CoPc.

The π bonds between the Cr ion and O induce the AFM couple between the Cr ion and the Co substrate. In contrast, the contribution of σ bonds was FM coupled. Thus, the total exchange energy between CrPc and the Co substrate was lower than that of MnPc. The results for FePc are like those of MnPc, and the exchange energy is higher than that of CrPc.

C. High SP for spintronic applications

The SP was one of the core factors to determine the material properties and device performance in spintronics [60–64]. The DOS of *M*Pcs on $c(2\times2)$O/Co(001) was plotted in Fig. 6. It was found that the DOS of all absorbed *M*Pcs showed magnetic metallic behavior owing to the hybridization with the surface oxidized Co. The SP was calculated by $\mathrm{SP} = (D_{\mathrm{up}} - D_{\mathrm{down}})/(D_{\mathrm{up}} + D_{\mathrm{down}}) \times 100\%$, where D_{up} and D_{down} are the spin-up and spin-down DOS at the Fermi level, respectively. The summary of SP for surface oxidized Co and *M*Pcs absorbed on the surface oxidized Co is shown in Table I. It is noted that the surface oxidized Co showed a positive SP about 45%, which was from the DOS of the O atoms on $c(2\times2)$O/Co(001) in Fig. S6 in the Supplemental Material [48]. Interestingly, the SPs of all adsorbed *M*Pcs were negative, agreeing with that of Co [26,64]. This indicates the adsorption of *M*Pcs reversed the SP of the surface oxidized Co. Most importantly, the SPs were up to −86% and −80% for CrPc and MnPc, respectively. Meanwhile, it was also found that the absorbed FePc and CoPc showed the SPs are −72% and −46%, respectively, which means the central atoms of *M*Pcs adjusted the SP by interface hybridization. Moreover, the high SPs of adsorbed *M*Pcs could maintain room temperature and benefit the application of *M*Pcs in spintronic devices because the magnetic coupling energy [see Fig. 1(c)] between Cr/Mn/Fe Pcs and the Co substrate was much higher than the thermal disturbance ($k_BT \sim 25$ meV) at room temperature. In addition, the surface of $c(2\times2)$O/Co(001) was achieved in experiments [34,46,47]. Particularly, it was demonstrated that the FePc is AFM coupled to the Co substrate via the O atomic layer [34], agreeing with the present results. The electric and magnetic properties of the spinterface for other *M*Pcs could also be explored using some advanced setups, such as scanning tunnel spectroscopy [4], x-ray absorption spectroscopy [7,9,34], and x-ray magnetic circular dichroism [10,11,25,34].

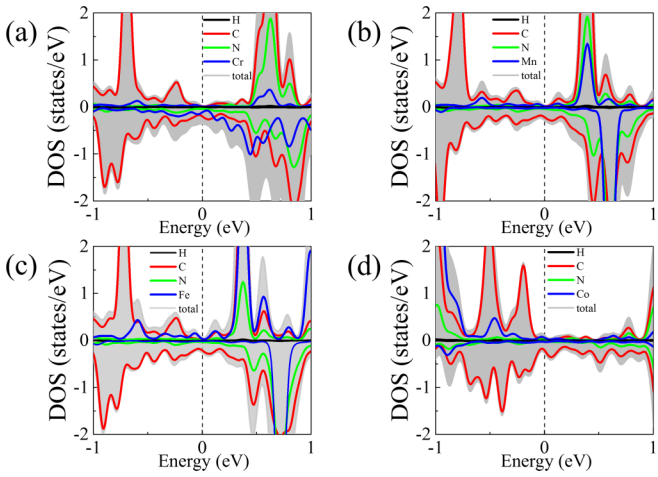

FIG. 6. Density of states (DOS) of *M*Pcs after absorbed on $c(2\times2)$O/Co(001). (a) DOS of CrPc. (b) DOS of MnPc. (c) DOS of FePc. (d) DOS of CoPc. The energy of Fermi energy was set to zero.

IV. CONCLUSIONS

This paper demonstrates that *M*Pcs (M = Cr, Mn, Fe, Co) are AFM coupled to the Co substrate through the interfacial O atomic layer, and the exchange strength strongly relies on

TABLE I. The spin polarizations (SPs) of the $c(2\times2)$O/Co(001) surface and absorbed *M*Pcs.

	O atoms on $c(2\times2)$O/Co(001)	CrPc	MnPc	FePc	CoPc
SP (%)	45	−86	−80	−72	−46

the central atoms of *M*Pcs. Both work function and adsorption energy were dominated by the magnitude of charge transfer between *M*Pcs and surface oxidized Co. Additionally, the valence and electron occupations of central 3*d* metal were changed by the adsorption, which was related to the exchange between *M*Pcs and the Co substrate. A superexchange model via O atoms was used to discuss the exchange between *M*Pcs and the Co substrate. The relatively high exchange energies of FePc and MnPc were due to the contribution of both π and σ bonds. As for CrPc, the offset of π and σ bonds reduced the exchange strength. The weak interaction between CoPc and the surface oxidized Co led to the weak exchange for CoPc through the σ bond. The SP of the spinterface was strongly related to the central metal of *M*Pcs. A high SP up to -86% was obtained in absorbed CrPc and could maintain room temperature due to the strong magnetic coupling, which could facilitate the application of *M*Pcs in spintronic devices. This means that the *M*Pcs could provide an effective way to adjust both electric and magnetic properties of the spinterface, which could be useful for applications of magnetic molecules in spintronics.

ACKNOWLEDGMENTS

This paper was supported by the National Natural Science Foundation of China (Grants No. 51971057 and No. 51675517), the Liaoning Revitalization Talents Program, and the Research Funds for the Central University (Grants No. N2002023 and No. N180206003).

There are no conflicts of interest to declare.

[1] M. Cinchetti, V. A. Dediu, and L. E. Hueso, Activating the molecular spinterface, Nat. Mater. **16**, 507 (2017).

[2] S. Lach, A. Altenhof, K. Tarafder, F. Schmitt, M. E. Ali, M. Vogel, J. Sauther, P. M. Oppeneer, and C. Ziegler, Metal-organic hybrid interface states of a ferromagnet/organic semiconductor hybrid junction as basis for engineering spin injection in organic spintronics, Adv. Funct. Mater. **22**, 989 (2012).

[3] J. Hu and R. Wu, Control of the Magnetism and Magnetic Anisotropy of a Single-Molecule Magnet with an Electric Field, Phys. Rev. Lett. **110**, 097202 (2013).

[4] N. Tsukahara, K.-I. Noto, M. Ohara, S. Shiraki, N. Takagi, Y. Takata, J. Miyawaki, M. Taguchi, A. Chainani, and S. Shin, Adsorption-Induced Switching of Magnetic Anisotropy in a Single Iron (II) Phthalocyanine Molecule on an Oxidized Cu (110) Surface, Phys. Rev. Lett. **102**, 167203 (2009).

[5] J. D. Baran, J. Larsson, R. A. Woolley, Y. Cong, P. J. Moriarty, A. A. Cafolla, K. Schulte, and V. R. Dhanak, Theoretical and experimental comparison of SnPc, PbPc, and CoPc adsorption on Ag (111), Phys. Rev. B **81**, 075413 (2010).

[6] J. Brede, N. Atodiresei, S. Kuck, P. Lazić, V. Caciuc, Y. Morikawa, G. Hoffmann, S. Blügel, and R. Wiesendanger, Spin-and Energy-Dependent Tunneling through a Single Molecule with Intramolecular Spatial Resolution, Phys. Rev. Lett. **105**, 047204 (2010).

[7] S. Javaid, M. Bowen, S. Boukari, L. Joly, J.-B. Beaufrand, X. Chen, Y. Dappe, F. Scheurer, J.-P. Kappler, and J. Arabski, Impact on Interface Spin Polarization of Molecular Bonding to Metallic Surfaces, Phys. Rev. Lett. **105**, 077201 (2010).

[8] T. Yu, Q. Zhang, D. Liu, and X. Han, Influence of organic layer thickness on structure, magnetic, and transport properties of Langmuir-Blodgett ttb-CuPc/CoFe, Appl. Phys. Lett. **102**, 022401 (2013).

[9] M. Gruber, F. Ibrahim, S. Boukari, H. Isshiki, L. Joly, M. Peter, M. Studniarek, V. Da Costa, H. Jabbar, and V. Davesne, Exchange bias and room-temperature magnetic order in molecular layers, Nat. Mater. **14**, 981 (2015).

[10] M. Gruber, F. Ibrahim, S. Boukari, L. Joly, V. Da Costa, M. Studniarek, M. Peter, H. Isshiki, H. Jabbar, and V. Davesne, Spin-dependent hybridization between molecule and metal at room temperature through interlayer exchange coupling, Nano Lett. **15**, 7921 (2015).

[11] G. Avvisati, C. Cardoso, D. Varsano, A. Ferretti, P. Gargiani, and M. G. Betti, Ferromagnetic and antiferromagnetic coupling of spin molecular interfaces with high thermal stability, Nano Lett. **18**, 2268 (2018).

[12] Y. Zhang, S. Du, and H.-J. Gao, Binding configuration, electronic structure, and magnetic properties of metal phthalocyanines on a Au (111) surface studied with *ab initio* calculations, Phys. Rev. B **84**, 125446 (2011).

[13] X. Zhang, J. Tong, L. Ruan, X. Yao, L. Zhou, F. Tian, and G. W. Qin, Interface hybridization and spin filter effect in metal-free phthalocyanine spin valves, Phys. Chem. Chem. Phys. **22**, 11663 (2020).

[14] M. Sun and W. Mi, Progress in organic molecular/ferromagnet spinterfaces: towards molecular spintronics, J. Mater. Chem. C **6**, 6619 (2018).

[15] T. L. A. Tran, D. Çakır, P. J. Wong, A. B. Preobrajenski, G. Brocks, W. G. van der Wiel, and M. P. de Jong, Magnetic properties of bcc-Fe(001)/C_{60} interfaces for organic spintronics, ACS Appl. Mater. Interfaces **5**, 837 (2013).

[16] S. Sanvito, Molecular spintronics: the rise of spinterface science, Nat. Phys. **6**, 562 (2010).

[17] N. Atodiresei, J. Brede, P. Lazić, V. Caciuc, G. Hoffmann, R. Wiesendanger, and S. Blügel, Design of the Local Spin Polarization at the Organic-Ferromagnetic Interface, Phys. Rev. Lett. **105**, 066601 (2010).

[18] F. Djeghloul, F. Ibrahim, M. Cantoni, M. Bowen, L. Joly, S. Boukari, P. Ohresser, F. Bertran, P. Le Fèvre, and P. Thakur, Direct observation of a highly spin-polarized organic spinterface at room temperature, Sci. Rep. **3**, 1 (2013).

[19] Z. Li, W. Mi, and H. Bai, Orbital redistribution enhanced perpendicular magnetic anisotropy of $CoFe_3N$ nitrides by adsorbing organic molecules, ACS Appl. Mater. Interfaces **10**, 16674 (2018).

[20] X. Han, W. Mi, and X. Wang, Spin polarization and magnetic properties at the $C_{60}/Fe_4N(001)$ spinterface, J. Mater. Chem. C **7**, 8325 (2019).

[21] X. Han, W. Mi, and D. Wang, Tunneling magnetoresistance and light modulation in $Fe_4N(La_{2/3}Sr_{1/3}MnO_3)/C_{60}/Fe_4N$ single

molecule magnetic tunnel junctions, J. Mater. Chem. C **8**, 3137 (2020).

[22] C. Barraud, K. Bouzehouane, C. Deranlot, D. Kim, R. Rakshit, S. Shi, J. Arabski, M. Bowen, E. Beaurepaire, and S. Boukari, Phthalocyanine based molecular spintronic devices, Dalton Trans. **45**, 16694 (2016).

[23] C. Barraud, P. Seneor, R. Mattana, S. Fusil, K. Bouzehouane, C. Deranlot, P. Graziosi, L. Hueso, I. Bergenti, and V. Dediu, Unravelling the role of the interface for spin injection into organic semiconductors, Nat. Phys. **6**, 615 (2010).

[24] T. Santos, J. Lee, P. Migdal, I. Lekshmi, B. Satpati, and J. Moodera, Room-Temperature Tunnel Magnetoresistance and Spin-Polarized Tunneling through an Organic Semiconductor Barrier, Phys. Rev. Lett. **98**, 016601 (2007).

[25] S. Boukari, H. Jabbar, F. Schleicher, M. Gruber, G. Avedissian, J. Arabski, V. Da Costa, G. Schmerber, P. Rengasamy, and B. Vileno, Disentangling magnetic hardening and molecular spin chain contributions to exchange bias in ferromagnet/molecule bilayers, Nano Lett. **18**, 4659 (2018).

[26] Z. Xiong, D. Wu, Z. V. Vardeny, and J. Shi, Giant magnetoresistance in organic spin-valves, Nature **427**, 821 (2004).

[27] C. Boehme and J. M. Lupton, Challenges for organic spintronics, Nat. Nanotechnol. **8**, 612 (2013).

[28] X. Zhang, S. Mizukami, T. Kubota, Q. Ma, M. Oogane, H. Naganuma, Y. Ando, and T. Miyazaki, Observation of a large spin-dependent transport length in organic spin valves at room temperature, Nat. Commun. **4**, 1392 (2013).

[29] K. V. Raman, Interface-assisted molecular spintronics, Appl. Phys. Rev. **1**, 031101 (2014).

[30] J. Tong, L. Ruan, X. Yao, G. Qin, and X. Zhang, Defect states dependence of spin transport in iron phthalocyanine spin valves, Phys. Rev. B **99**, 054406 (2019).

[31] J. M. Coey, *Magnetism and Magnetic Materials* (Cambridge University Press, New York, 2010), Chaps. 4 and 5.

[32] T. Kroll, R. Kraus, R. Schönfelder, V. Y. Aristov, O. Molodtsova, P. Hoffmann, and M. Knupfer, Transition metal phthalocyanines: insight into the electronic structure from soft x-ray spectroscopy, J. Chem. Phys **137**, 054306 (2012).

[33] H. C. Herper, S. Bhandary, O. Eriksson, B. Sanyal, and B. Brena, Fe phthalocyanine on Co (001): influence of surface oxidation on structural and electronic properties, Phys. Rev. B **89**, 085411 (2014).

[34] D. Klar, B. Brena, H. Herper, S. Bhandary, C. Weis, B. Krumme, C. Schmitz-Antoniak, B. Sanyal, O. Eriksson, and H. Wende, Oxygen-tuned magnetic coupling of Fe-phthalocyanine molecules to ferromagnetic Co films, Phys. Rev. B **88**, 224424 (2013).

[35] I. E. Brumboiu, S. Haldar, J. Lüder, O. Eriksson, H. C. Herper, B. Brena, and B. Sanyal, Influence of electron correlation on the electronic structure and magnetism of transition-metal phthalocyanines, J. Chem. Theory Comput. **12**, 1772 (2016).

[36] M.-S. Liao and S. Scheiner, Electronic structure and bonding in metal phthalocyanines, metal = Fe, Co, Ni, Cu, Zn, Mg, J. Chem. Phys **114**, 9780 (2001).

[37] A. Mugarza, R. Robles, C. Krull, R. Korytár, N. Lorente, and P. Gambardella, Electronic and magnetic properties of molecule-metal interfaces: transition-metal phthalocyanines adsorbed on Ag (100), Phys. Rev. B **85**, 155437 (2012).

[38] G. Kresse and J. Furthmüller, Efficiency of *abinitio* total energy calculations for metals and semiconductors using a plane-wave basis set. Comput. Mater. Sci. **6**, 15 (1996).

[39] G. Kresse and J. Furthmüller, Efficient iterative schemes for *ab initio* total-energy calculations using a plane-wave basis set, Phys. Rev. B **54**, 11169 (1996).

[40] J. P. Perdew, K. Burke, and M. Ernzerhof, Generalized Gradient Approximation Made Simple, Phys. Rev. Lett. **77**, 3865 (1996).

[41] J. Girovsky, K. Tarafder, C. Wäckerlin, J. Nowakowski, D. Siewert, T. Hählen, A. Wäckerlin, A. Kleibert, N. Ballav, and T. A. Jung, Antiferromagnetic coupling of Cr-porphyrin to a bare Co substrate, Phys. Rev. B **90**, 220404(R) (2014).

[42] S. Grimme, Semiempirical GGA-type density functional constructed with a long-range dispersion correction, J. Comput. Chem. **27**, 1787 (2006).

[43] V. Wang, N. Xu, J. C. Liu, G. Tang, and W.-T. Geng, VASPKIT: a user-friendly interface facilitating high-throughput computing and analysis using VASP code, arXiv:1908.08269.

[44] C. Li, A. J. Freeman, and C. Fu, Electronic structure and surface magnetism of fcc Co (001), J. Magn. Magn. Mater **75**, 53 (1988).

[45] G. P. Pun and Y. Mishin, Embedded-atom potential for hcp and fcc cobalt, Phys. Rev. B **86**, 134116 (2012).

[46] X. Liu, T. Iimori, K. Nakatsuji, and F. Komori, Invasive growth of Co on $(\sqrt{2} \times 2\sqrt{2})R45^{\circ}$ reconstructed O/Cu (001), Appl. Phys. Lett. **88**, 133102 (2006).

[47] C. Sorg, N. Ponpandian, M. Bernien, K. Baberschke, H. Wende, and R. Wu, Induced magnetism of oxygen in surfactant-grown Fe, Co, and Ni monolayers, Phys. Rev. B **73**, 064409 (2006).

[48] See Supplemental Material at https://link.aps.org/supplemental/10.1103/PhysRevB.103.024435 for energies of different adsorption configurations, spin-charge density, mechanism model of superexchange, and density of states of O atoms.

[49] J. Tong, L. Ruan, X. Yao, F. Tian, G. Qin, and X. Zhang, Unexpected magnetic coupling oscillations for $L1_0$-MnGa/Co(Fe) films induced by quantum wells, Phys. Rev. B **97**, 184426 (2018).

[50] W. Tang, E. Sanville, and G. Henkelman, A grid-based Bader analysis algorithm without lattice bias, J. Phys. Condens. Matter **21**, 084204 (2009).

[51] G. Henkelman, A. Arnaldsson, and H. Jónsson, A fast and robust algorithm for Bader decomposition of charge density, Comput. Mater. Sci. **36**, 354 (2006).

[52] E. Sanville, S. D. Kenny, R. Smith, and G. Henkelman, Improved grid-based algorithm for Bader charge allocation, J. Comput. Chem. **28**, 899 (2007).

[53] S. Gueddida and M. Alouani, Calculated impact of ferromagnetic substrate on the spin crossover in a Fe(1, 10-phenanthroline)$_2$(NCS)$_2$ molecule, Phys. Rev. B **93**, 184433 (2016).

[54] Y.-P. Wang, X.-F. Han, Y.-N. Wu, and H.-P. Cheng, Adsorption of tris (8-hydroxyquinoline) aluminum molecules on cobalt surfaces, Phys. Rev. B **85**, 144430 (2012).

[55] S. Javaid, S. Lebègue, B. Detlefs, F. Ibrahim, F. Djeghloul, M. Bowen, S. Boukari, T. Miyamachi, J. Arabski, and D. Spor, Chemisorption of manganese phthalocyanine on Cu (001) surface promoted by van der Waals interactions, Phys. Rev. B **87**, 155418 (2013).

[56] S. Peljhan and A. Kokalj, Adsorption of chlorine on Cu (111): a density-functional theory study, J. Phys. Chem. C **113**, 14363 (2009).

[57] J. Zuckerman, Crystal field splitting diagrams, J. Chem. Educ. **42**, 315 (1965).

[58] P. W. Anderson, New approach to the theory of superexchange interactions, Phys. Rev. **115**, 2 (1959).

[59] E. Koch, Lecture notes of the Autumn School correlated electrons 2012, in *Correlated Electrons: From Models to Materials*, edited by E. Pavarini, E. Koch, F. Anders, and M. Jarrell (Autumn School, Jülich, 2012), Vol. 2.

[60] M. Julliere, Tunneling between ferromagnetic films, Phys. Lett. A **54**, 225 (1975).

[61] V. Garcia, M. Bibes, L. Bocher, S. Valencia, F. Kronast, A. Crassous, X. Moya, S. Enouz-Vedrenne, A. Gloter, and D. Imhoff, Ferroelectric control of spin polarization, Science **327**, 1106 (2010).

[62] J. Tong, F. Luo, L. Ruan, L. Zhou, F. Tian, G. Qin, and X. Zhang, High and reversible spin polarization in a collinear antiferromagnet, Appl. Phys. Rev. **7**, 031405 (2020).

[63] B. Yang, L. Tao, L. Jiang, W. Chen, P. Tang, Y. Yan, and X. Han, Ultrahigh Tunneling-Magnetoresistance Ratios in Nitride-Based Perpendicular Magnetic Tunnel Junctions from First Principles, Phys. Rev. Appl. **9**, 054019 (2018).

[64] J. P. Velev, K. D. Belashchenko, D. A. Stewart, M. van Schilfgaarde, S. Jaswal, and E. Y. Tsymbal, Negative Spin Polarization and Large Tunneling Magnetoresistance in Epitaxial Co|$SrTiO_3$|Co Magnetic Tunnel Junctions, Phys. Rev. Lett. **95**, 216601 (2005).